Non-standard Thermal Histories
and Temperature of the Universe

Patrick Brown

I. ACKNOWLEDGEMENTS

II. ABSTRACT

Non-standard thermal histories have recently attracted significant attention due to a combination of experimental and theoretical considerations. In a well-motivated class of models the universe went through an epoch of early matter domination (EMD) before it was one second old. The standard scenario of EMD involves on species whose equation of state is the same as that of non-relativistic matter. Here, we consider a generalized scenario where EMD is driven by a large number of such species.

We will start by setting up a system of coupled Boltzmann equations that govern evolution of the radiation energy density in generalized EMD. Then we will consider two explicit examples that involve a large number of modulus fields and a population of small primordial black holes (PBHs) respectively. We will find the temperature of the universe during EMD by numerically solving the system of Boltzmann equations and also provide analytical approximations in both cases. Our main conclusion is that the generalized EMD scenario includes a long intermediate stage during which the temperature behaves very differently from that in the standard scenario of EMD. This can have very important consequences for production of dark matter (DM) relic abundance.

III. INTRODUCTION

Cosmology has evolved into a precise experimental science over the past few decades. The influx of high quality data from various observations, made possible by advances in technology, has led to the emergence of the "Standard Model of Cosmology" that describes the universe and its evolution to the present state based on only a few parameters. According to the standard cosmological model, also known as "ΛCDM, the energy budget of the universe at the present time is roughly 5% matter, 25% DM, and 70% dark energy [1]. This model successfully describes evolution of tiny density fluctuations of $\mathcal{O}(10^{-5})$ in the early universe, found imprinted in temperature anisotropy of the cosmic microwave background (CMB), into structures such as galaxies and galaxy clusters. The dominant paradigm for explaining primordial density fluctuations is a brief period of superluminal expansion of the early universe called "inflation" [2]. Transition from inflation to hot big bang that leads to establishment of a thermal bath of elementary particle is called "reheating"[3].

In a "standard thermal history," shortly after inflation ends the universe enters a radiation-dominated (RD) phase of thermalized relativistic particles, which persists for

$\sim 50,000$ years when a matter-dominated (MD) era begins (called "matter-radiation equality"). This provides an attractive and predictive picture that allows the use of systems of Boltzmann equations to follow processes among particles in the thermal bath until they become inefficient (i.e., the rate for a given process becomes smaller than the expansion rate of the universe). In regards to DM [4] this gives rise to a scenario where the DM relic abundance is set when annihilation of DM particles to ordinary particles ceases to be efficient. The correct DM abundance can be obtained within this scenario for weakly interacting massive particles (WIMPs) as DM candidate, hence called "WIMP miracle."

Despite being simple and predictive, there is no direct observational evidence for the standard thermal history. Currently, primordial synthesis of light nuclei, called big bang nucleosynthesis (BBN) [5], is our best direct probe of the earliest moments of the universe. Agreements between BBN predictions and observations indicate that the universe was indeed in a RD phase when it was one second old. However, observations do not give us information about the state of the universe at much earlier times. Moreover, from the theory side, there are well-motivated particle physics models of the early universe that predict a non-standard thermal history [6]. In these models the universe goes through an early phase similar to MD, hence "early matter domination" (EMD), that ends prior to the onset of BBN. An epoch of EMD can have important cosmological implications, notably for alternative mechanisms of DM production [7].

Therefore, experimental and theoretical considerations motivate studying non-standard thermal histories and their cosmological consequences. The proposed research aims at investigating issues in this direction with a particular emphasis on an EMD phase and temperature of the universe in such an era.

An epoch of EMD typically arises in non-standard thermal histories. This epoch is driven by species behaving like non-relativistic matter (so that pressure basically vanishes). In order to establish a RD universe before BBN occurs, this phase must end well before the universe is one second old. By taking the exponential decay of unstable species to radiation into account, one can solve a system of equations that govern the evolution of energy densities in matter and radiation. After using the well-known relation between the energy density of radiation and its temperature $\rho_r = (\pi^2/30)g_* T^4$, where g_* denotes the number of relativistic degrees of freedom, it can be shown that during EMD temperature evolves differently from that in a RD universe [8]. As a consequence, production of DM particles during EMD proceeds very differently form that in RD. In particular, a period of EMD opens up large parts of the parameter where the correct DM relic abundance can be obtained [9].

In the standard picture, EMD is driven by the energy density of a single species with zero pressure, which is typically coherent oscillations of a scalar field that arises in extensions of the "Standard Model of Particle Physics." Realistic models, however, contain more than one of such species. For example, models motivated by string theory include a number of modulus fields that can undergo coherent oscillations in the early universe [6]. Also, models based on supersymmetry include a large number of scalar fields that can lead to coherent oscillations in specific directions in their field space [10]. Moreover, it is possible to have other species in the early universe that behave like matter such as PBHs [11]. A population of small PBHs may form shortly after inflation ends and decay to radiation and DM before BBN [12].

The goal of this research is to investigate situations where the EMD phase is driven by more than a single species and to study evolution of the temperature of the universe during EMD in these situations. After a brief review the standard EMD scenario, we will

consider the simplest case where two species (for example, two scalar fields undergoing coherent oscillations) are responsible for EMD. We will find the temperature in this case by numerically solving the system of equations that govern evolution of the energy densities of these species and radiation. Next, we will consider a general situation where a population of species within a continuous mass range with a distribution function $\beta(m)$ drives the EMD. We will first set up the system of equations that govern the evolution of these species and their decay into radiation. We will then specialize to two physically motivated cases: (1) a population of modulus fields, and (2) a population of PBHs.

IV. NOTE

All theoretical and numerical calculations in this paper are calculated using natural units and the reduced Plank Mass:

$$\hbar = k = c = 1$$

$$M_p = 2.4 * 10^{18} GeV$$

$$1.52 * 10^{24} s^{-1} = 1 GeV$$

V. EARLY MATTER DOMINATION: THE STANDARD SCENARIO

We will start with the standard EMD scenario that involves a single species. This case is described by the following Boltzmann equations whose complete derivation is discussed in Kolb and Turner:

$$
\begin{aligned}
&\frac{d\rho_1}{dt} + 3H\rho_1 = -\Gamma_1\rho_1\,, \\
&\frac{d\rho_r}{dt} + 4H\rho_r = \Gamma_1\rho_1\,, \\
&\frac{da}{dt} = aH\,, \\
&H = \left(\frac{\rho_r + \rho_1}{3M_P^2}\right)^{1/2}\,.
\end{aligned}
\tag{1}
$$

Here the subscript 1 represents the species behaving like matter, the subscript r represents radiation, H denotes the Hubble expansion rate, a is the scale factor of the universe, and M_P is the reduced Plank Mass.

The system of equations is solved using MatLab and the built in ode15s (or the ode45) differential equation solver. This solver is a variation on the Runga-Kutta method and is specifically built to handle steeply changing functions. The reason we use this solver (and the ode45 solver) is because after the matter field has decayed to the point where the energy densities of matter and radiation are equal, the density of matter drops off rapidly as it is decaying into radiation in an exponential manner. This quick drop off is too difficult for most solvers to handle and can cause interference with results concerning the final radiation density that produce incorrect behavior. The ode15s and ode45 solvers are built to handle this and more information is available on the MatLab website.

The graph of the matter energy density, radiation energy density, and the total energy density as a function of the scale factor (normalized to its initial value) is shown in section nine figure one. The decay rate is $\Gamma_1 = 10^{-9} H_0$, where the initial Hubble expansion rate follows $H_0^2 = \rho_0/3M_P^2$. The temperature can be obtained from ρ_r using the the well known relation:

$$\boxed{\rho_r = \frac{g_* \pi^2 T^4}{30}} (E.1)$$

mentioned before, and its graph is shown in section nine figure two.

For $\Gamma \ll H \ll H_0$, we can find an analytic expression for T. In this regime, $4H\rho_r$ term can be neglected. Furthermore, ρ_1 mainly changes due to the expansion of the universe as the decay is in its initial stages, which implies $\rho \propto a^{-3}$.

Plugging this relation into the radiation energy density equation, we find:

$$\frac{d\rho_r}{dt} \propto \frac{\Gamma_1}{a^3}. \tag{2}$$

From the definition of the Hubble expansion rate $H = da/adt$, we can write $dt = da/aH$. After using the fact that in a MD phase $H \propto a^{-3/2}$, we arrive at:

$$\frac{d\rho_r}{da} \propto \Gamma_1 a^{-5/2}. \tag{3}$$

Integrating this equation over da, and using $\rho_r \propto T^4$, we find:

$$\boxed{T \propto a^{-3/8}} (E.2) \tag{4}$$

This well-known scaling of T with a [8] is observed in the temperature graph above. Contrasting it with the scaling relation:

$$\boxed{T \propto a^{-1}} (E.3)$$

due to Hubble expansion alone, we see that temperature during EMD decreases more slowly than in a RD phase. This can be intuitively understood as follows: while during RD temperature decreases due to expansion only, in EMD decay of unstable species to radiation partially compensates the effect of expansion.

A simple extension of the standard scenario involves two matter species decaying into radiation. In this case the system of Boltzmann equations is:

$$\frac{d\rho_1}{dt} + 3H\rho_1 = -\Gamma_1\rho_1 \,,$$
$$\frac{d\rho_2}{dt} + 3H\rho_2 = -\Gamma_2\rho_2 \,,$$
$$\frac{d\rho_r}{dt} + 4H\rho_r = \Gamma_1\rho_1 + \Gamma_2\rho_2 \,,$$
$$\frac{da}{dt} = aH \,,$$
$$H = \left(\frac{\rho_r + \rho_1 + \rho_2}{3M_P^2}\right)^{1/2} \,. \tag{5}$$

These equations are solved once again using ode45 resulting in figure three of section nine (assuming the two species have the same initial energy density). The temperature distribution is shown in figure four of section nine.

The notable feature is that temperature scales as $T \propto a^{-3}$ for $H \gg \Gamma_1$ and $\Gamma_2 \ll H \ll \Gamma_1$, but decreases more steeply in the intermediate regime (for a detailed discussion, see [13]). This shows that adding one more species to the standard scenario can significantly affect evolution of the temperature during the EMD epoch.

VI. THE CONTINUUM LIMIT

Before moving onto the explicit examples analyzed, we consider the continuum limit where the EMD epoch is driven by a continuous distribution of species over a mass range. The complete set of Boltzmann equations in the continuum limit are:

$$
\frac{d\beta(m)}{dt} + 3H\beta(m) = -\Gamma(m)\beta(m) \,,
$$
$$
\frac{d\rho_r}{dt} + 4H\rho_r = \int_{m_{min}}^{m_{max}} \Gamma(m)\beta(m)dm \,,
$$
$$
H = \left(\frac{\rho_r + \int_{m_{min}}^{m_{max}} \beta(m)dm}{3M_P^2} \right)^{1/2} \,. \tag{6}
$$

Multiplying the first equation by a^3 results in the following expression for $\beta(m)$:

$$
\beta(m) = \frac{\beta_0(m)a_0^3}{a^3}e^{-\Gamma_m t}. \tag{7}
$$

In order to obtain analytical approximations for ρ_r and T, we need more information about $\beta_0(m)$ and $\Gamma(m)$. Here we consider two well-motivated cases that we have studied in the explicit examples discussed below.

1. Modulus fields

Moduli are scalar fields that arise in models based on string theory [6]. Their value at the minimum of their potential determine the volume and shape of extra spatial dimensions. They are typically displaced from their minimum during inflation and thereby acquire a non-zero energy density. The initial energy density of a modulus field with mass m is $\sim m^2 M_P^2$. It starts oscillating about the minimum of its potential when the Hubble expansion rate drops below m. The coherent oscillations of a massive scalar field behave like non-relativistic particles of mass m [8].

In the case of many modulus fields, their initial energy density scales with their mass as m^2. They start out oscillating one after another (from the heaviest to the lightest). It can be shown that when all of the modulus fields have started oscillating, thus behaving like matter, they have the same energy density. This implies an initially flat distribution $\beta_0(m) = \text{const.}$ in the continuum limit. Moreover, the decay rate of a modulus field of mass m is given by:

$$\Gamma(m) \simeq \frac{m^3}{2\pi M_P^2}. \tag{8}$$

Plugging these into the equation for radiation energy density in (6), and multiplying both sides by a^4, we find:

$$a^4 \rho_r = \frac{\beta_0 a_0^3}{M_P^2} \int a(t) \int_{m_{min}}^{m_{max}} m^3 e^{\frac{-m^3 t}{M_P^2}} dt dm. \tag{9}$$

Making a change of variable $u = m^3 t/M_P^2$ gives:

$$a^4 \rho_r = \beta_0 a_0^3 \int a(t) \int_{m_{min}}^{m^{max}} M_P^{2/3} t^{-4/3} u^{1/3} e^{-u} du dt. \tag{10}$$

We can write ρ_r in terms of the incomplete gamma functions:

$$\rho_r = \frac{\beta_0 a_0^3 M_P^{2/3}}{a^4} \int a(t) t^{-4/3} [\gamma(\frac{4}{3}, \frac{m_{max}^3 t}{M_P^2}) - \gamma(\frac{4}{3}, \frac{m_{min}^3 t}{M_P^2})] dt. \tag{11}$$

In order to evaluate this integral, we must make some approximations. We can find an analytic approximation for temperature within the time interval $\Gamma_{m_{max}}^{-1}) \ll t\Gamma_{m_{min}}^{-1}$ during EMD, where we can set $m_{max}^3 t/M_P^2 \to \infty$ in the first gamma function and $m_{min}^3 t/M_P^2 \to 0$ in the second one. This leads to:

$$\rho_r \sim \frac{\beta_0 a_0^3 M_P^{2/3} \Gamma(\frac{4}{3})}{a^4} \int a(t) t^{-4/3} dt, \tag{12}$$

which, after using the relation $a \propto t^{2/3}$ during EMD, becomes:

$$\rho_r \sim \frac{\beta_0 a_0^3 M_P^{2/3} \Gamma(\frac{4}{3}) t^{1/3}}{a^4}. \tag{13}$$

We then arrive at the following scaling relation for temperature:

$$\boxed{T \propto a^{-7/8}} (E.4), \tag{14}$$

which is significantly different from that in the standard EMD scenario (4). The physical interpretation of this difference has to do with the fact that moduli heavier than $\sim (t M_P^2)^{1/3}$ have already decayed at time t while the lighter ones are still around.

During the earlier stages of EMD when $t \ll \Gamma_{m_{max}}^{-1}$, the integral in (12) yields the relation $T \propto a^{-3/8}$. This is the same as the standard scenario, which is expected since all of the modulus fields are still present at such early times. At late times when $t \gg \Gamma_{m_{min}}^{-1}$, the integral yields $T \propto a^{-1}$, which is also expected because all of moduli have already decayed and T only changes because of Hubble expansion.

2. Primordial Black Holes

There are two main differences between this case and that for modulus fields. First, a PBH with mass m evaporates via Hawking radiation at a rate:

$$\Gamma(m) = \frac{\pi M_P^4}{80m^3}. \tag{15}$$

Second, as pointed out in [12], a reasonable choice for the initial distribution function of PBHs is $\beta(m) \propto m^{-1}$. Taking into account these differences, and by repeating the same steps as in the case of moduli, we derive the following relation between T and a during EMD driven by PBHs when $\Gamma_{m_{max}}^{-1} \ll t \ll \Gamma_{m_{min}}^{-1}$:

$$\boxed{T \propto a^{-3/4}} (E.5) \tag{16}$$

At early times $t \ll \Gamma_{m_{max}}^{-1}$ and late times $t \gg \Gamma_{m_{min}}^{-1}$ we find $T \propto a^{-3/8}$ and T^{-1}, respectively, similar to the previous case.

VII.   FIRST EXPLICIT EXAMPLE: A LARGE NUMBER OF MODULUS FIELDS

We have have included 10,000 modulus fields uniformly distributed within the mass range $M_{min} = 10^4 GeV$ to $M_{max} = 10^8 GeV$ with equal initial energy densities (to follow the physically motivated behavior $\beta(m) = $ const. in the continuum limit). The relevant system of Boltzmann equations in this case is:

$$\frac{d\rho_i}{dt} + 3H\rho_i = -\Gamma_i \rho_i \,,$$

$$\frac{d\rho_r}{dt} + 4H\rho_r = \sum_{i=1}^{N} \Gamma_i \rho_i \,,$$

$$\frac{da}{dt} = aH \,,$$

$$H = \left(\frac{\rho_r + \sum_{i=1}^{N} \rho_i}{3M_P^2} \right)^{1/2} . \tag{17}$$

Here ρ_i's denote 10,000 modulus fields ($N = 10,000$) with respective masses m_i and decay rates $\Gamma_i \simeq m_i^3/2\pi M_P^2$.

We have solved these equations in MatLab, using the the ode45 solver. The radiation energy density ρ_r, total energy density in moduli $\sum_i \rho_i$, and total energy density $\rho_{tot} = \rho_r + \sum_i \rho_i$ during EMD are shown in section nine figure five. The graph for temperature distribution of the universe during this EMD scenario is shown in section nine figure six.

We can see three distinct phases in these figures. The first phase occurs for $a \sim 1 - 10^2$ (where the scale factor a is normalized to its initial value a_0). During this phase, which we can call the "memory phase", no appreciable amount of radiation is produced by by decay of modulus fields and the initial radiation energy density is simply redshifted due to Hubble expansion. As a result, $T \propto a^{-1}$ (E.3) that is clearly seen in the temperature graph. The second phase corresponds to the range $a \sim 10^2 - 10^8$. In this phase none of the moduli have completely decayed yet, and hence the situation is similar to that in the standard EMD scenario where $T \propto a^{-3/8}$ (E.2). The third phase corresponds to the range $a \sim 10^8 - 10^{17}$, during which some of the modulus fields have completely decayed while the rest are still

present. In this phase we can use the analytical approximation discussed in the continuum $T \propto a^{-7/8}$ (E.4), which is in good agreement with the slope seen in the temperature graph. Finally, at $a \sim 10^{17}$ a RD universe is established after all of the modulus fields have decayed during which $T \propto a^{-1}$ (E. 3).

VIII.   SECOND EXPLICIT EXAMPLE: A LARGE NUMBER OF PRIMORDIAL BLACK HOLES

We have chosen 10,000 PBHs uniformly distributed over the mass range $M_{min} = 7 * 10^{24} GeV$ to $M_{max} = 2*10^{32} GeV$ with the initial energy densities proportional to the inverse of mass (to follow the physically motivated behavior $\beta(m) \propto m^{-1}$ in the continuum limit). The system of Boltzmann equations in this case is the same as that in the previous case (17). However, the evaporation rate Γ_i of the PBH with mass m_i is given by $\Gamma_i = \pi M_P^4/80m_i^3$.

We have again solved these equations in MatLab, using ode45 solver. The graph for various energy densities and for temperature during EMD are shown in section nine figures seven and eight.

In this case, the initial radiation energy density is negligible, and hence there is no "memory phase" at the beginning. We see that $T \propto a^{-3/8}$ (E. 2) for $a \sim 10^0 - 10^3$ and $a \sim 10^8 - 10^9$, similar to the standard EMD, with an intervening phase were $T \propto a^{-1}$ (E. 3). This is different from the case of moduli and it is due to the fact that the lightest PBH that evaporates first also carries the largest fraction of energy density. Its evaporation therefore leads to injection of a significant amount of radiation that is then redshifted due to Hubble expansion. In a sense, the phase corresponding to $a \sim 10^3 - 10^9$ may be called the "memory phase" from evaporation of the lightest PBH. We expect this phase to become shorter with increasing the number of PBHs and eventually vanish in the continuum limit. For $a \sim 10^9 - 10^{17}$, some of the PBHs have evaporated while the rest are still present. In this phase we can use the analytical approximation in the continuum limit $T \propto a^{-3/4}(E.5)$, see Eq. (P.5). Finally, at $a \sim 10^{17}$ the entire population of PBHs have evaporated and the universe enters a RD phase during which $T \propto a^{-1}$ (E. 3).

IX.   CONCLUSIONS AND FUTURE WORK

Non-standard thermal histories of the early universe are motivated on theoretical grounds and typically involve an epoch of EMD. In this work we have generalized the standard picture of EMD that involves only one species behaving like non-relativistic matter. We have studied two explicit examples that arise in realistic particle physics models of the early universe where EMD is driven by a population of modulus fields and PBHs respectively.

We considered the continuum limit of both cases and obtained analytical approximations for temperature of the universe during the generalized EMD. Our novel result is that for long periods of time temperature decreases significantly differently from that in the standard scenario. We confirmed our analytical results by numerically solving the relevant system of Boltzmann equations for a large number of modulus fields and PBHs.

Our results have important implications for production of DM in the early universe. It is known that the standard EMD scenario significantly enlarges the allowed regions of parameter space that yield the observed DM abundance [9]. It has been recently shown that a simple extension of the standard scenario that involves a second field opens up large

parts of the parameter space [13]. We can therefore expect that entirely new regions of the parameter space become viable in the generalized EMD scenario. To tackle this problem, one must solve equations for production of DM from processes in the thermal bath along with the system of Boltzmann equation that govern evolution of radiation, which is in general very involved. However, the importance of the origin of DM abundance for cosmology and particle physics warrants a detailed investigation along this direction in future.

---

[1] N. Aghanim *et al.* [Planck Collaboration], e-Print: arXiv:1807.06209 [astro-ph.CO].

[2] For a review, see: A. D. Linde, Contemp. Concepts Phys. **5**, 1 (1990) [e-Print: hep-th/0503203]].

[3] For a review, see: R. Allahverdi, R. Brandenberger, F-Y Cyr-Racine and A. Mazumdar, Ann. Rev. Nucl. Part. Sci. **60**, 27 (2010) [e-Print: arXiv:1001.2600 [hep-th]].

[4] For a review, see: G. Bertone, D. Hooper and J. Silk, Phys. Rept. **405**, 279 (2005) [e-Print: hep-ph/0404175].

[5] For a review, see: K. A. Olive, G. Steigman and T. P. Walker, Phys. Rept. **333**, 389 (2000) [e-Print: astro-ph/9905320].

[6] For a review, see: G. Kane, K. Sinha and S. Watson, Int. J. Mod. Phys. D **24**, 1530022 (2015) [e-Print: arXiv:1502.07746 [hep-th]].

[7] H. Baer, K.Y. Choi, J. E. Kim and L. Roszkowski, Phys. Rept. **555**, 1 (2015) [e-Print: arXiv:1407.0017 [hep-ph]].

[8] For example, see: E. W. Kolb and M. S. Turner, "The Early Universe", Addison-Wesley (1990).

[9] G. F. Giudice, E. W. Kolb and A. Riotto, Phys. Rev. D **64**, 023508 (2001) [e-Print: hep-ph/0005123].

[10] I. Affleck and M. Dine, Nucl. Phys. B **249**, 361 (1985).

[11] B. J. Carr and S. W. Hawking, Mon. Not. Roy. Astron. Soc. **168**, 399 (1974).

[12] R. Allahverdi, J. Dent and J. Osinski, Phys. Rev. D **97**, 055013 (2018) [e-Print: arXiv:1711.10511 [astro-ph.CO]].

[13] R. Allahverdi and J. Osinski, Phys. Rev. D **99**, 083517 (2019) [e-Print: arXiv:1812.10522 [hep-ph]].

X. FIGURES
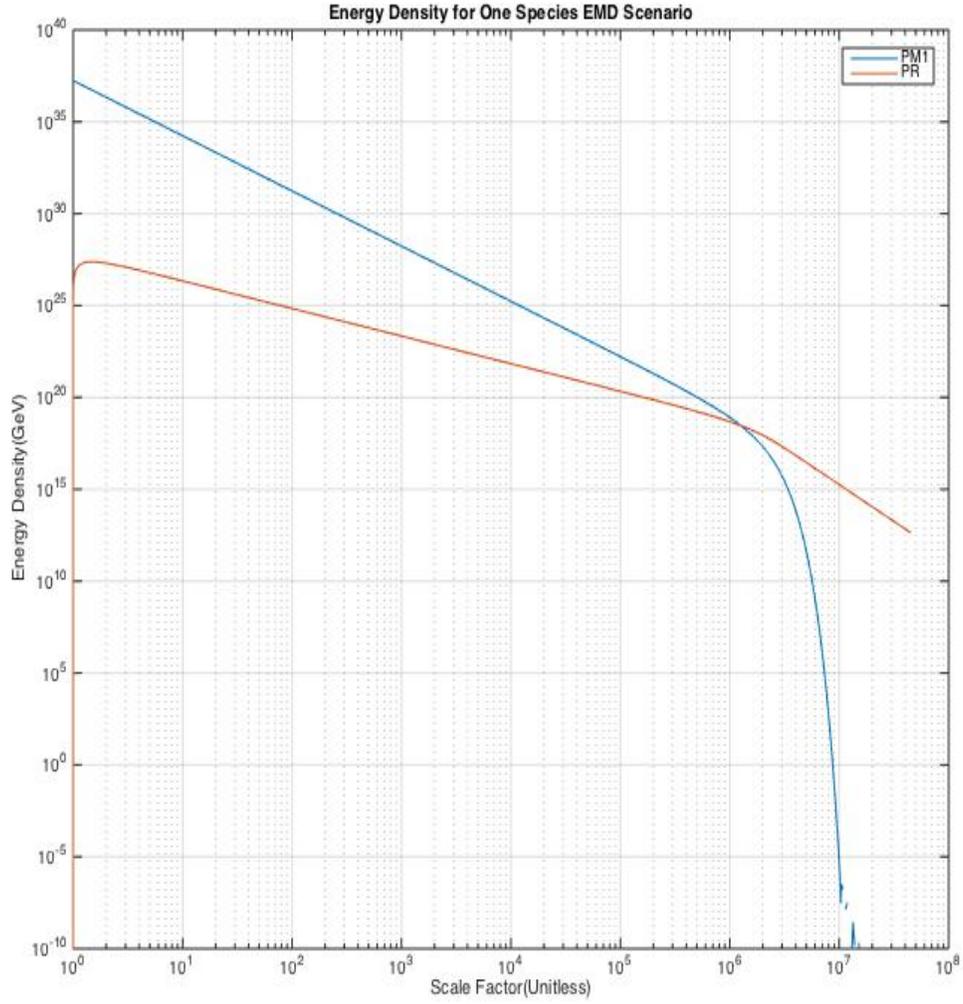
FIG. 1: Graph of radiation and matter energy densities for one field scenario. The x-axis is the scale factor a and is normalized to unit-less. The y-axis is the energy density and is measured in GeV. The blue is the matter field and the red is the radiation field. The initial matter energy density is $\rho_i = 3(M_P * H_0)^2 (GeV)$, the decay rate is $\frac{\Gamma_1}{H_o} = 10^{-9}$, and the initial radiation energy density is $\rho_r = 10^{-10}(GeV)$.
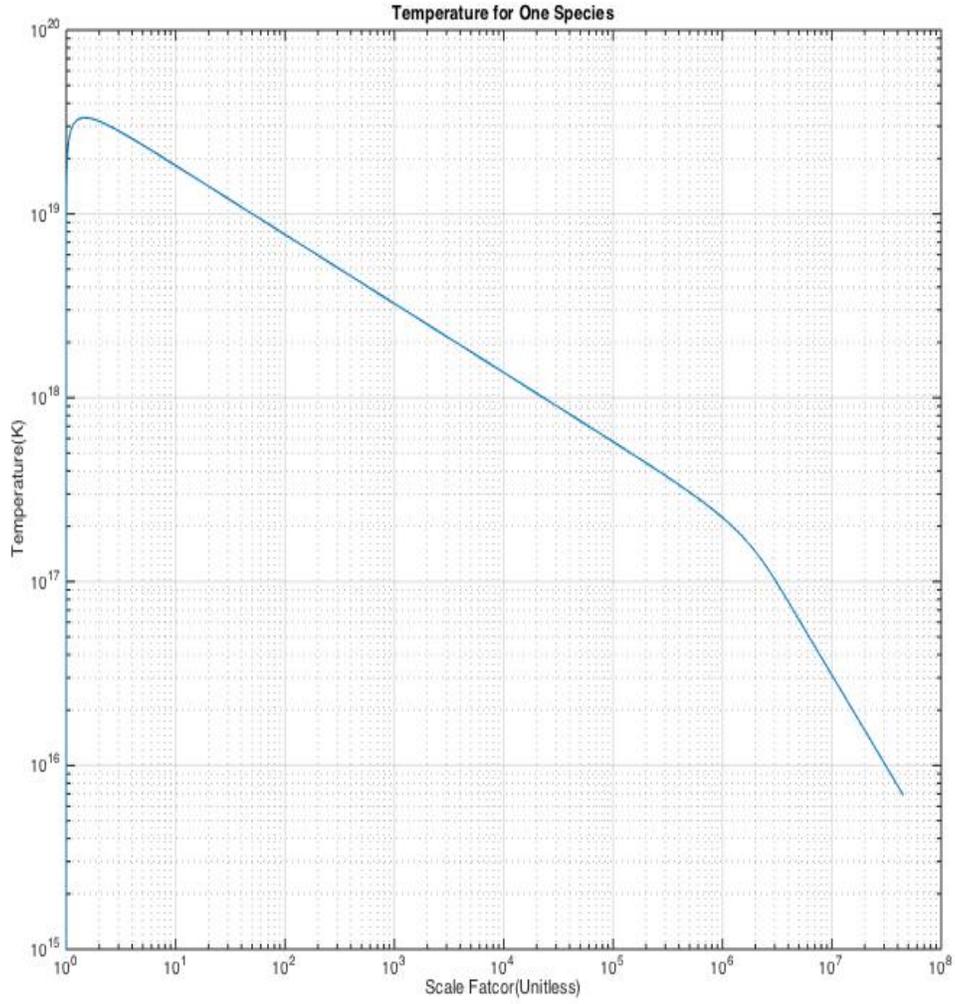
FIG. 2: Graph of temperature distribution of early universe for the one field scenario. The x-axis is the scale factor a and is normalized to unit-less. The y-axis is the temperature measured in Kelvin.
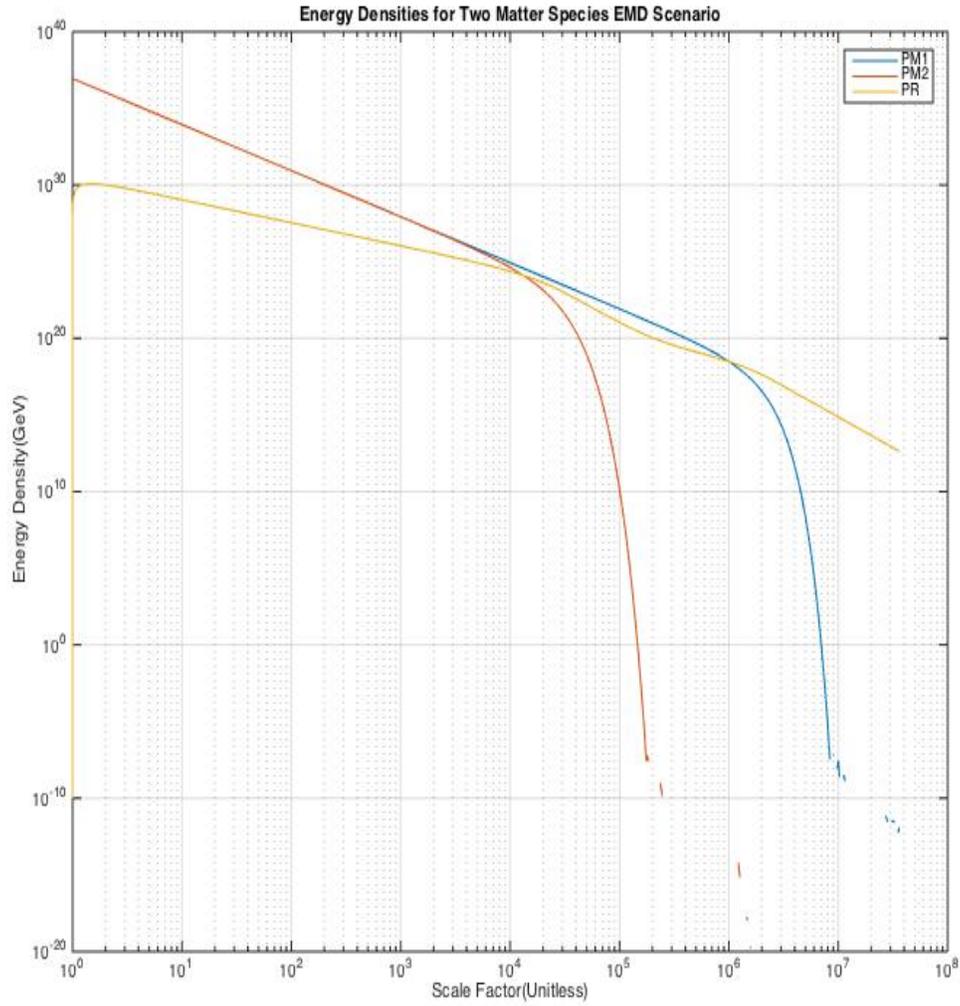
FIG. 3: Graph of radiation and matter energy densities for two field scenario. The x-axis is the scale factor a and is normalized to unit-less. The y-axis is the energy density and is measured in GeV. The blue and red are the matter fields; and the yellow is the radiation field. The initial matter energy density is $\rho_i = \frac{3(M_P * H_0)^2}{2}(GeV)$, the decay rates are $\frac{\Gamma_1}{H_o} = 10^{-9}(sec^{-1})$ and $\frac{\Gamma_2}{H_o} = 10^{-6}(GeV)$, and the initial radiation energy density is $\rho_r = 10^{-10}(GeV)$.
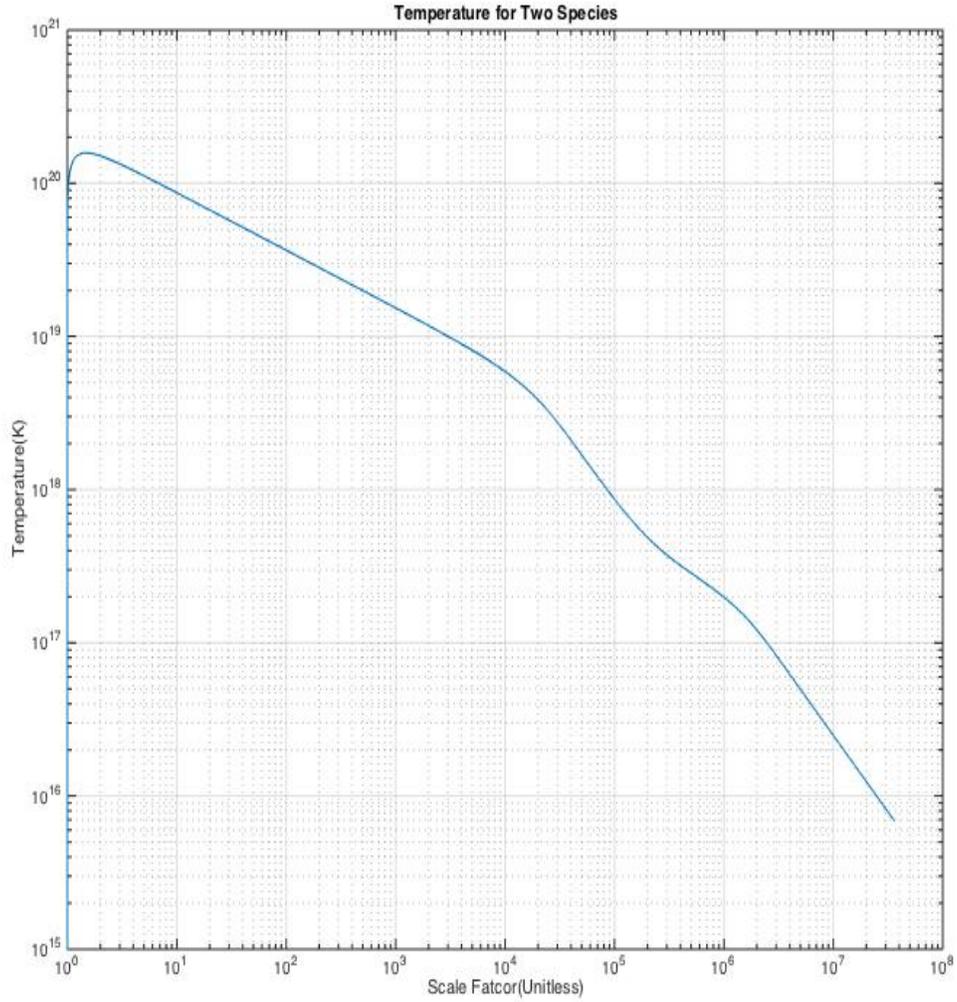
FIG. 4: Graph of temperature distribution of early universe for the two field scenario. The x-axis is the scale factor a and is normalized to unit-less. The y-axis is the temperature measured in Kelvin.
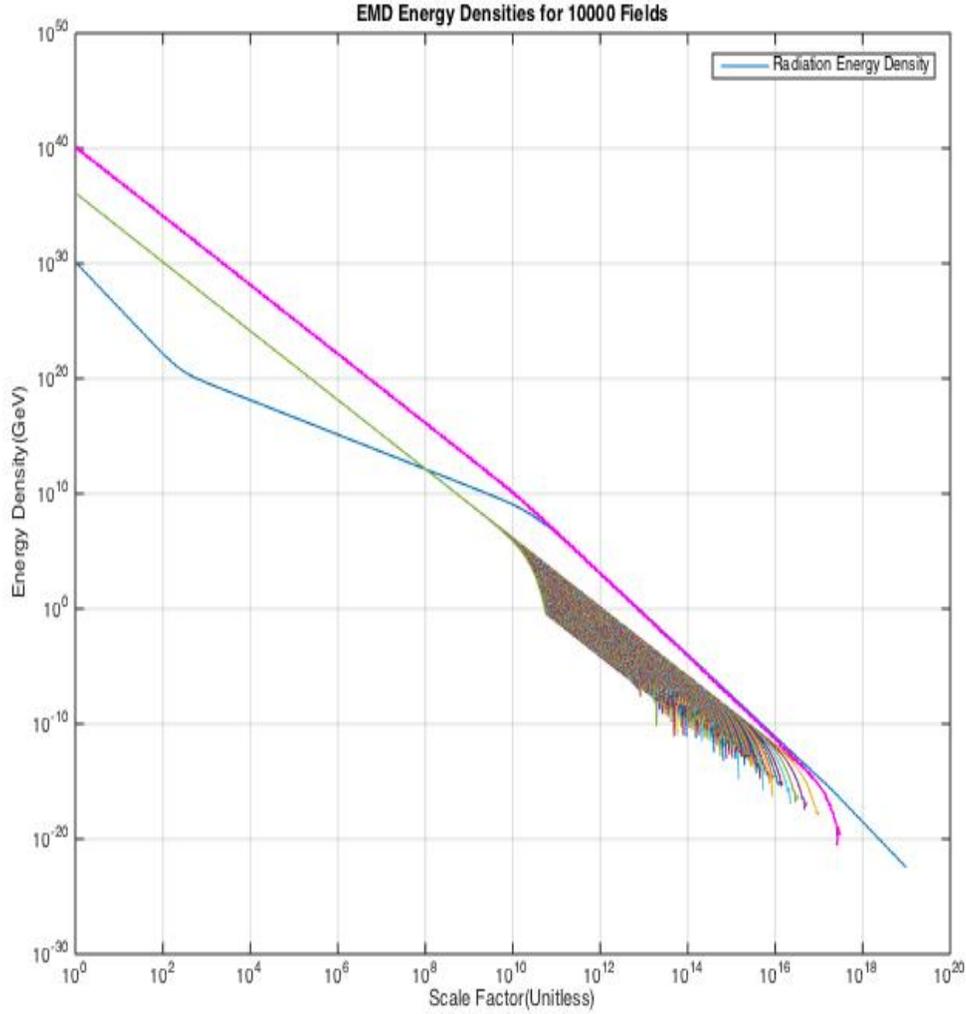
FIG. 5: Graph of radiation and matter energy densities for the N modulus fields scenario. The x-axis is the scale factor a and is normalized to unit-less. The y-axis is the energy density and is measured in GeV. The blue is the radiation field, the magenta is the total sum of the matter energy densities, and the other colors are the individual matter fields . The initial matter energy density is $\rho_i = \frac{3(M_P * H_0)^2}{N}(GeV)$, the decay rates are $\Gamma_i = \frac{m^3}{2\pi M_P^2}(GeV)$, and the initial radiation energy density is $\rho_r = 10^{-10}(GeV)$. The memory phase follows $T \propto a^{-1}$ (E.3), the second phase follows $T \propto a^{-3/8}$ (E.2), the third phase follows $T \propto a^{-7/8}$ (E.4), and the fourth phase follows $T \propto a^{-1}$ (E. 3).
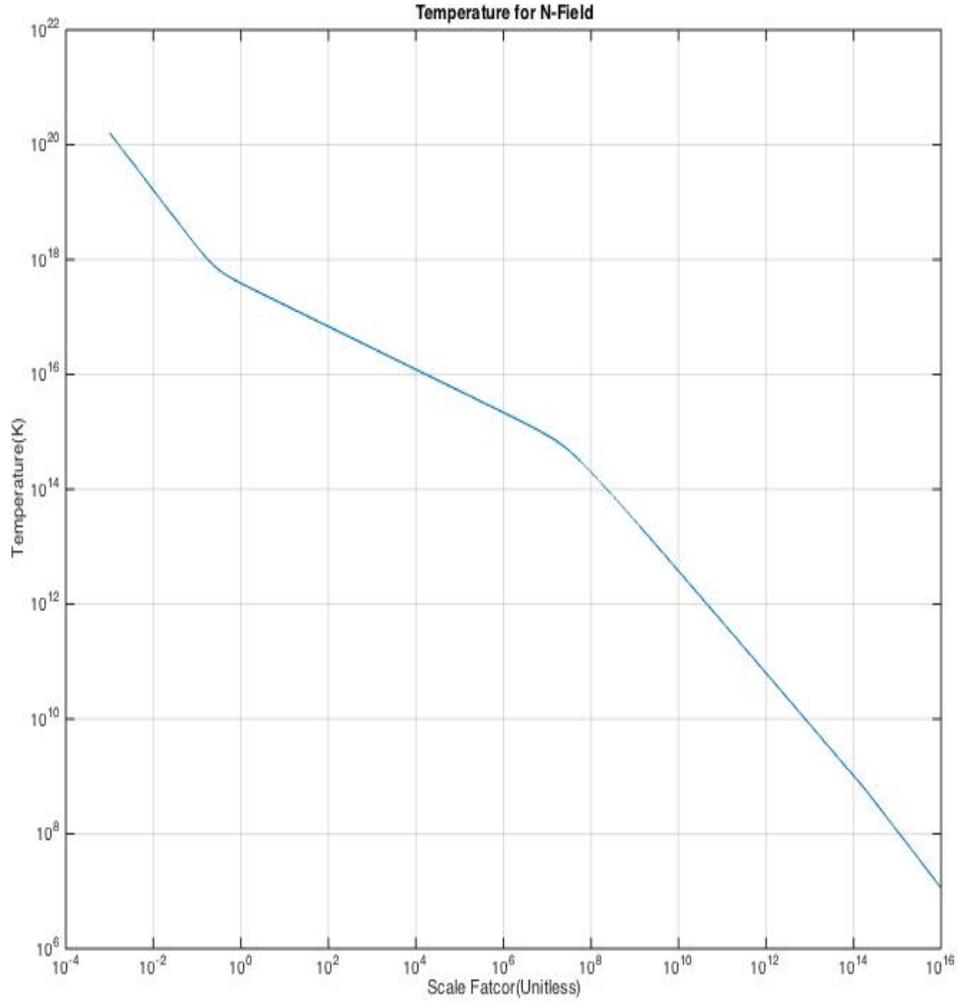
FIG. 6: Graph of temperature distribution of early universe for the N modulus field scenario. The x-axis is the scale factor a and is normalized to unit-less. The y-axis is the temperature measured in Kelvin. The memory phase follows $T \propto a^{-1}$ (E.3), the second phase follows $T \propto a^{-3/8}$ (E.2), the third phase follows $T \propto a^{-7/8}$ (E.4), and the fourth phase follows $T \propto a^{-1}$ (E. 3).
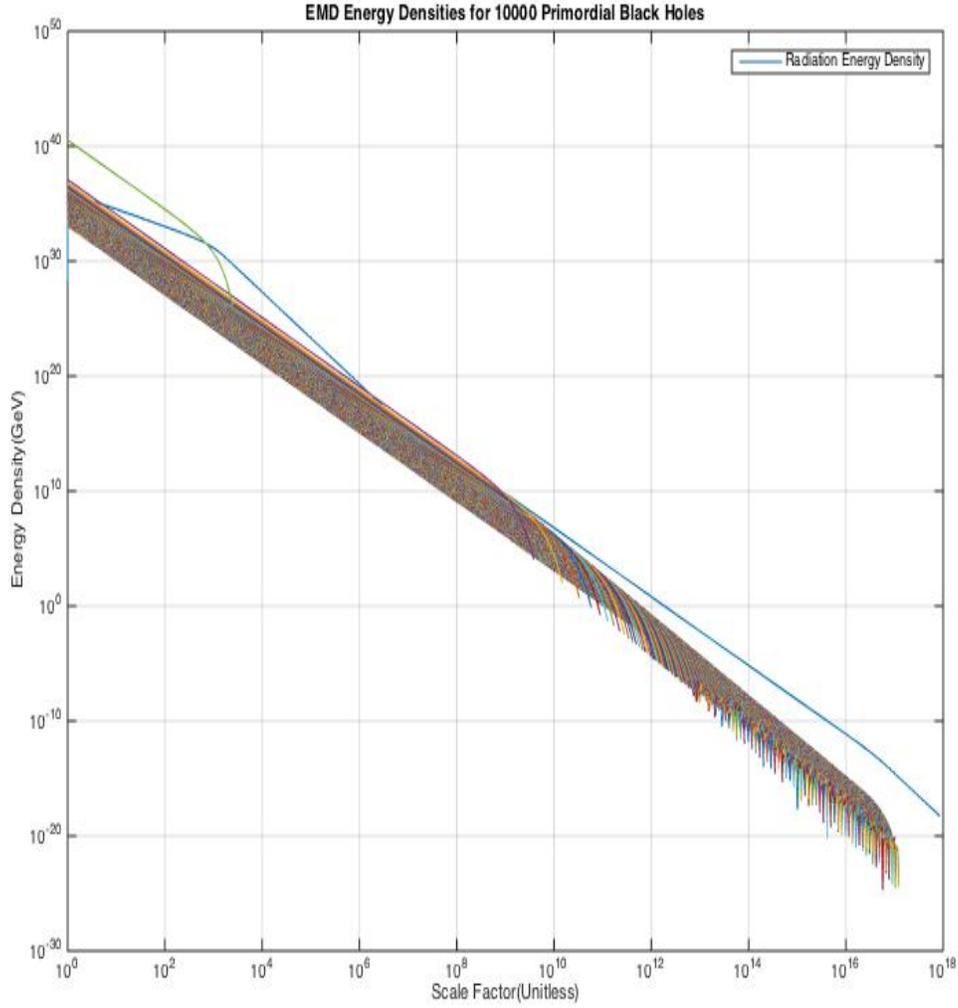
FIG. 7: Graph of radiation and matter energy densities for the N primordial black hole scenario. The x-axis is the scale factor a and is normalized to unit-less. The y-axis is the energy density and is measured in GeV. The blue is the radiation field and the other colors are the individual matter fields . The initial matter energy density is $\rho_i = \frac{3(M_P * H_0)^2}{m} dm (GeV)$ where dm is the step size for the mass distribution, the decay rates are $\Gamma_i = \frac{\pi M_P^3}{80m^4} (sec^{-1})$, and the initial radiation energy density is $\rho_r = 10^{-10} (GeV)$. The first phase follows $T \propto a^{-3/8}$ (E. 2), the intervening phase follows $T \propto a^{-1}$ (E. 3), the second phase follows $T \propto a^{-3/4}$ (E.5), and the third phase follows $T \propto a^{-1}$ (E. 3).
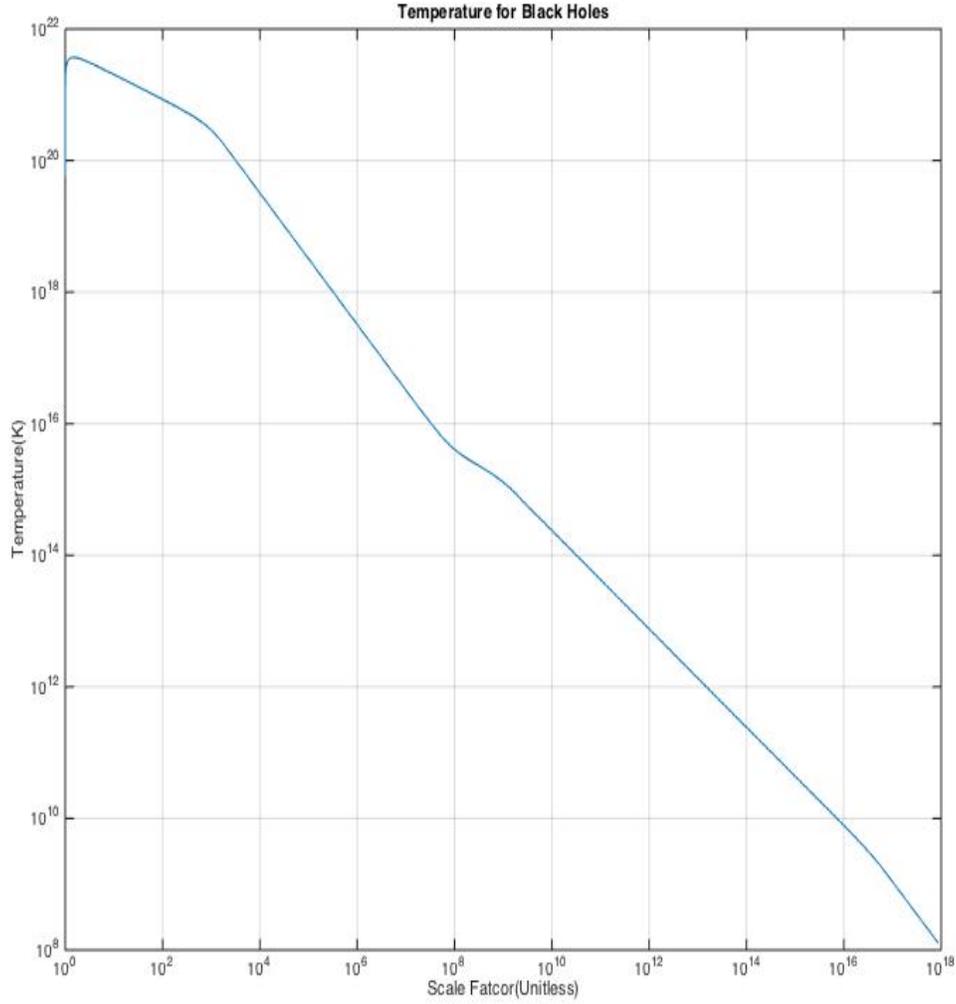
FIG. 8: Graph of temperature distribution of early universe for the N primordial black hole scenario. The x-axis is the scale factor a and is normalized to unit-less. The y-axis is the temperature measured in Kelvin. The first phase follows $T \propto a^{-3/8}$ (E. 2), the intervening phase follows $T \propto a^{-1}$ (E. 3), the second phase follows $T \propto a^{-3/4}$ (E.5), and the third phase follows $T \propto a^{-1}$ (E. 3).